speeds due to greater viscosity differences in an upper mantle operating at a reasonable Rayleigh number (~10^6; ref. 17). □

Received 14 February; accepted 10 October 2000.

1. White, R. S. *et al.* Magmatism at rifted continental margins. *Nature* **330,** 439–444 (1987).
2. White, R. S. & McKenzie, D. P. Magmatism at rift zones: the generation of volcanic continental margins and flood basalts. *J. Geophys. Res.* **94,** 7685–7729 (1989).
3. Jones, E. J. W., Ramsay, A. T. S., Preston, N. J. & Smith, A. C. S. A Cretaceous guyot in the Rockall Trough. *Nature* **251,** 129–131 (1974).
4. Jones, E. J. W., Siddall, R., Thirwall, M. F., Chronston, P. N. & Lloyd, A. J. Anton Dohrn Seamount and the evolution of the Rockall Trough. *Oceanol. Acta* **17,** 237–247 (1994).
5. Dietrich, R. V. & Jones, E. J. W. Volcanic rocks from Rosemary Bank (Rockall Trough, NE Atlantic). *Mar. Geol.* **35,** 287–297 (1980).
6. Saunders, A. D., Fitton, J. G., Kerr, A. C., Norry, M. J. & Kent, R. W. in *Large Igneous Provinces: Continental, Oceanic, and Planetary Flood Volcanism* (eds Mahoney, J. J. & Coffin, M. F.) 45–93 (Geophysical Monograph 100, American Geophysical Union, Washington DC, 1997).
7. Kerr, A. C. The melting processes and composition of the North Atlantic (Iceland) plume: geochemical evidence from the Early Tertiary basalts. *J. Geol. Soc. Lond.* **152,** 975–978 (1995).
8. Fram, M. S., Lesher, C. E. & Volpe, A. M. Mantle melting systematics: Transition from continental to oceanic volcanism on the southeast Greenland margin. *Proc. ODP Sci. Res.* **152,** 373–386 (1998).
9. Mussett, A. E. & McCormack, A. G. *Magnetic Polarity Timescales: a New Test* 27–37 (Special Publication 70, Geological Society, London, 1992).
10. Pearson, D. G., Emeleus, C. H. & Kelley, S. P. Precise $^{40}Ar/^{39}Ar$ age for the initiation of Palaeogene volcanism in the Inner Hebrides and its regional significance. *J. Geol. Soc. Lond.* **153,** 815–818 (1996).
11. Hamilton, M. A., Pearson, D. G., Thompson, R. N., Kelley, S. P. & Emeleus, C. H. Rapid eruption of Skye lavas inferred from precise U-Pb and Ar-Ar dating of the Rum and Cuillin plutonic complexes. *Nature* **394,** 260–263 (1998).
12. Sinton, C. W. & Duncan, R. A. ^{40}Ar-^{39}Ar ages of lavas from the southeast Greenland margin, ODP Leg 152, and the Rockall Plateau, DSDP Leg 81. *Proc. ODP Sci. Res.* **152,** 387–402 (1998).
13. Tegner, C. *et al.* ^{40}Ar-^{39}Ar geochronology of Tertiary mafic intrusions along the East Greenland rifted margin: Relation to flood basalts and the Iceland hotspot track. *Earth Planet. Sci. Lett.* **156,** 75–88 (1998).
14. Storey, M., Duncan, R. A., Pedersen, A. K., Larsen, L. M. & Larsen, H. C. $^{40}Ar/^{39}Ar$ geochronology of the West Greenland Tertiary volcanic province. *Earth Planet. Sci. Lett.* **160,** 569–586 (1998).
15. Tegner, C. & Duncan, R. A. ^{40}Ar-^{39}Ar chronology for the volcanic history of the southeast Greenland rifted margin. *Proc. ODP Sci. Res.* **163,** 53–62 (1999).
16. Richards, M. A., Duncan, R. A. & Courtillot, V. E. Flood basalts and hot-spot: Plume heads and tails. *Science* **246,** 103–107 (1989).
17. Larsen, T. B., Yuen, D. A. & Storey, M. Ultrafast mantle plumes and implications for flood basalt volcanism in the Northern Atlantic Region. *Tectonophysics* **311,** 31–43 (1999).
18. Larsen, H. C. & Saunders, A. D. Tectonism and volcanism at the southeast Greenland rifted margin: A record of plume impact and later continental rupture. *Proc. ODP Sci. Res.* **152,** 503–533 (1998).
19. Mussett, A. E., Dagley, P. & Skelhorn, R. R. *Time and Duration of Activity in the British Tertiary Igneous Province* 337–348 (Special Publication 39, Geological Society, London, 1988).
20. Meighan, I. G., McCormick, A. G., Gibson, D., Gamble, J. A. & Graham, I. J. *Rb-Sr Isotopic Determinations and the Timing of Tertiary Central Complex Magmatism in NE Ireland* 349–360 (Special Publication 39, Geological Society, London, 1988).
21. Upton, B. G. J., Emeleus, C. H., Rex, D. C. & Thirwall, M. F. Early Tertiary magmatism in NE Greenland. *J. Geol. Soc. Lond.* **152,** 959–964 (1995).
22. Vogt, P. R. Asthenosphere motion recorded by the ocean floor south of Iceland. *Earth Planet. Sci. Lett.* **13,** 153–160 (1971).
23. White, R. S., Brown, J. W. & Smallwood, J. R. The temperature of the Iceland plume and the origin of outward-propagating V-shaped ridges. *J. Geol. Soc. Lond.* **152,** 1039–1045 (1995).
24. White, N. & Lovell, B. Measuring the pulse of a plume with the sedimentary record. *Nature* **387,** 888–891 (1997).
25. Hanan, B. B. & Schilling, J.-G.The dynamic evolution of the Iceland mantle plume: the lead isotope perspective. *Earth Planet. Sci. Lett.* **151,** 43–60 (1997).
26. Larsen, T. B. & Yuen, D. A. Ultrafast upwelling bursting through the upper mantle. *Earth Planet. Sci. Lett.* **146,** 393–399 (1997).
27. Bijwaard, H. & Spakman, W. Tomographic evidence for a narrow whole mantle plume below Iceland. *Earth Planet. Sci. Lett.* **166,** 121–126 (1998).
28. Kent, R. W., Storey, M. & Saunders, A. D. Large igneous provinces: Sites of plume impact or plume incubation? *Geology* **20,** 891–894 (1992).
29. Clague, D. A. & Dalrymple, G. B. in *The Eastern Pacific Ocean and Hawaii: The Geology of North America* (eds Winterer, E. L., Hussong, D. M. & Decker, R. W.) 187–286 (Geological Society of America, Boulder, Colorado, 1989).
30. O'Connor, J. M., Stoffers, P. & Wijbrans, J. R. Migration rate of volcanism along the Foundation Chain, SE Pacific. *Earth Planet. Sci. Lett.* **164,** 41–59 (1998).
31. *GEBCO Digital Atlas* (British Oceanographic Data Centre, Bidston, 1997).
32. Morton, A. C. *et al.* Late Cretaceous basalts from Rosemary Bank, Northern Rockall Trough. *J. Geol. Soc. Lond.* **152,** 947–952 (1995).

Supplementary information is available on *Nature*'s World-Wide Web site (http://www.nature.com) or as paper copy from the London editorial office of *Nature*.

Acknowledgements

We thank Captain Gross and the crew of FS *Poseidon,* along with the scientific party, for ship handling and support during sampling, and T. Arpe and D. Garbe-Schoenberg for ICP-MS data. LDEO supplied a Rosemary bank rock sample. J.O'C. was affiliated to AWI-Bremerhaven during much of this study. This work was supported by the DFG.

Correspondence and requests for information should be addressed to J.O'C. (e-mail: joconnor@geomar.de).

Subduction and collision processes in the Central Andes constrained by converted seismic phases

X. Yuan*†, S. V. Sobolev*, R. Kind*†, O. Oncken*†, G. Bock*‖, G. Asch*‖, B. Schurr*‖, F. Graeber*‖, A. Rudloff*‖, W. Hanka*‖, K. Wylegalla*‖, R. Tibi*‖, Ch. Haberland†‖, A. Rietbrock†‖, P. Giese†‖, P. Wigger †‖, P. Röwer†‖, G. Zandt‡‖, S. Beck‡‖, T. Wallace‡‖, M. Pardo§‖ & D. Comte§‖

** GeoForschungsZentrum Potsdam, Telegrafenberg, 14473 Potsdam, Germany*
† Freie Universität Berlin, Fachrichtung Geophysik, Malteser Str. 74-100, 12249 Berlin, Germany
‡ University of Arizona, Department of Geosciences, Tucson, Arizona 85721, USA
§ Universidad de Chile, Departemento de Geofisico, Blanco Encalada 2085, Santiago, Chile
‖ Andes Working Group

The Central Andes are the Earth's highest mountain belt formed by ocean–continent collision[1,2]. Most of this uplift is thought to have occurred in the past 20 Myr, owing mainly to thickening of the continental crust[2–6], dominated by tectonic shortening[7–10]. Here we use P-to-S (compressional-to-shear) converted teleseismic waves observed on several temporary networks in the Central Andes to image the deep structure associated with these tectonic processes. We find that the Moho (the Mohorovičić discontinuity—generally thought to separate crust from mantle) ranges from a depth of 75 km under the Altiplano plateau to 50 km beneath the 4-km-high Puna plateau. This relatively thin crust below such a high-elevation region indicates that thinning of the lithospheric mantle may have contributed to the uplift of the Puna plateau. We have also imaged the subducted crust of the Nazca oceanic plate down to 120 km depth, where it becomes invisible to converted teleseismic waves, probably owing to completion of the gabbro–eclogite transformation; this is direct evidence for the presence of kinetically delayed metamorphic reactions in subducting plates. Most of the intermediate-depth seismicity in the

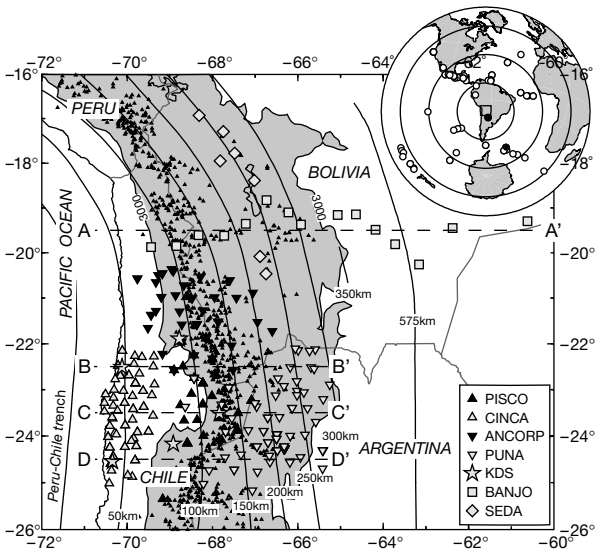

Figure 1 Map of the Central Andes, showing networks of passive seismological stations used in this study. Areas with elevation higher than 3 km are shaded. Contour lines mark the Wadati–Benioff zone[27]. Small triangles mark volcanoes. Inset, locations of several teleseismic earthquakes and two deep regional earthquakes used in this study. Data from two earthquakes marked by filled circles show strong P-to-S conversions of the subducted Nazca plate, and are modelled in Fig. 4.

subducting plate stops at 120 km depth as well, suggesting a relation with this transformation. We see an intracrustal low-velocity zone, 10–20 km thick, below the entire Altiplano and Puna plateaux, which we interpret as a zone of continuing metamorphism and partial melting that decouples upper-crustal imbrication from lower-crustal thickening.

The Central Andes are a unique place where subduction and mountain-building processes can be studied, both in their extremes. Whereas subduction has been continuing at least since the early Mesozoic era, evolution of the Andean cordillera has been concentrated in the Cenozoic era during continuous subduction of the Nazca plate under the Central Andes at a velocity between 6 and 15 cm yr^{-1} (refs 1, 2). The Moho of the continental upper plate has been detected by different seismic methods at 30–80 km depth, with its deepest parts below the Eastern and Western Cordilleras, which border the Altiplano and Puna plateaux[3–6]. The altitude of the plateaux (about 4 km) has been explained as an isostatic response to crustal thickening[2,6]. A low average P-wave velocity and low Poisson's ratio in the crust of the northern Altiplano have been reported from seismic observations, indicating tectonic shortening as the dominant mechanism of crustal thickening in the northern Central Andes[5,6]. Geological studies, however, report only up to 250 km of crustal shortening (equivalent to some 70% of the width of the Altiplano[7–9]) and only some 75 km of shortening at the latitude of Puna[10]. Our aim was to resolve crustal and mantle structures associated with the plateau building and subduction processes in the Central Andes.

Several seismic networks were operated between 1994 and 1997 in northern Chile, southern Bolivia and northwestern Argentina (Fig. 1) for periods ranging from two months to one year. Receiver functions (RFs) (P-to-S converted waves isolated from the incident teleseismic P waves) are commonly used to constrain crustal velocities and to detect crustal and upper-mantle discontinuities underneath seismic stations[11,12]. Figure 2a shows the first 15 s after P onset of about 500 averaged RFs displayed on an east–west profile between 65° and 71° W. Besides the strong phases marked B (at less than 1 s) and M (at 6–8 s), which are conversions from the basement and the Moho, there are some other pronounced intracrustal phases that can be traced across the entire Altiplano and Puna. They are called trans-Andean converters (TRAC) and in Fig. 2 are marked TRAC1 (blue, negative, velocity decrease downwards) and TRAC2 (red, positive, velocity increase downwards). The subducting Nazca plate is also visible.

As a dense seismic network is available, it is helpful to migrate the RFs into the space domain to image seismic discontinuities[13,14]—a process similar to the near-vertical incidence reflection method in crustal studies. Figure 2c shows, as background to an interpretative cartoon, the time domain RFs of Fig. 2a migrated into a depth domain image of the crust and upper mantle of the Central Andes down to 200 km depth. The most pronounced feature in Fig. 2a and c is the continental Moho converter at 40–75 km depth. It is consistent with the previous estimates of crustal thickness in the Central Andes from seismological observations[5,6] and from wide-angle reflections[4]. Images of the Moho along four lines crossing the Central Andes (see Fig. 1 for location of lines) are presented in Fig. 3

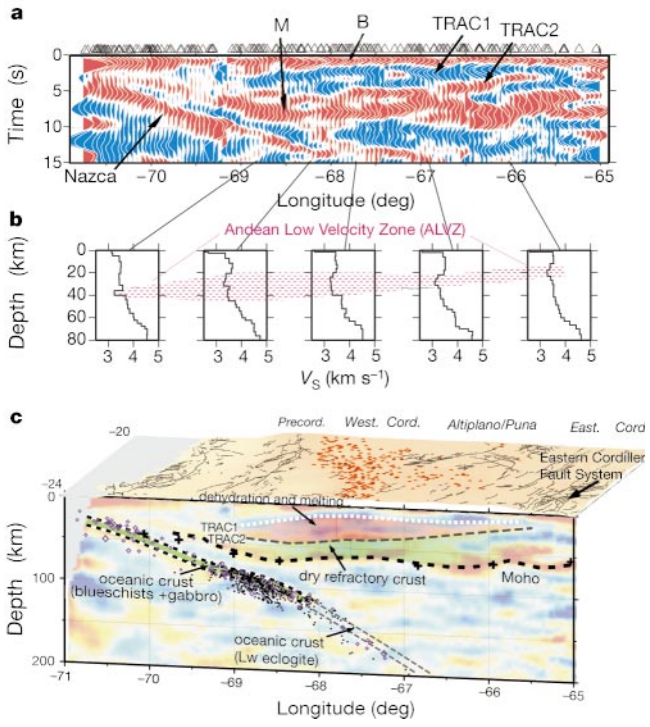

Figure 2 Receiver function (RF) images and crustal models of the Central Andes along an east–west profile. In the images, red indicates positive, velocity increase downwards; blue indicates negative, velocity reduction downwards. **a**, Time domain RFs averaged over a 30-km-wide moving window, 2–10-s band pass filtered. **b**, Possible crustal S-wave velocity (v_S) models resulting from the inversion of the RFs in **a**. **c**, Interpretative cartoon with depth-migrated RF image as background averaged over the Altiplano and Puna regions. Black plus signs show Moho depth data from wide-angle reflection studies[4]. Local crustal models and a global mantle reference model were used for migration. The TRAC1 and TRAC2 converters in **a** and **c** border the Andean low-velocity zone (ALVZ) which dips westwards from below the Eastern Cordillera fault system (indicated in **c** by black lines at the surface) across the entire Altiplano/Puna to the Precordillera (red points at surface indicate Cenozoic volcanoes). Figure S1 in Supplementary Information shows this data set split in two at 23° S for judging north–south variations of the TRAC2 converter. Figure S2 in Supplementary Information shows the lateral extension of the ALVZ. The Nazca converter (thick black-white dashed line indicated in **c**) is interpreted as an image of the oceanic Moho. The upper boundary of the oceanic crust (slab shear zone) is set 10 km above the oceanic Moho in agreement with the results of waveform inversion (see text and Fig. 4). Oceanic crust is clearly visible from converted waves only down to 120 km depth. Hypocentres of the intermediate depth earthquakes are also shown. Black dots are small-magnitude events ($M = 2–4$) located by the PISCO network during 3 months of operation[28]. Purple diamonds are 1965–95 relocated events[29] at 22–24° S, with the depth corrected for the local velocity model in the Central Andes. Only the best located events that have more than 10 depth phases are shown. Their magnitudes, ranging from 4.5 to 6.5, are indicated by the symbol size. Lw, the mineral lawsomite.

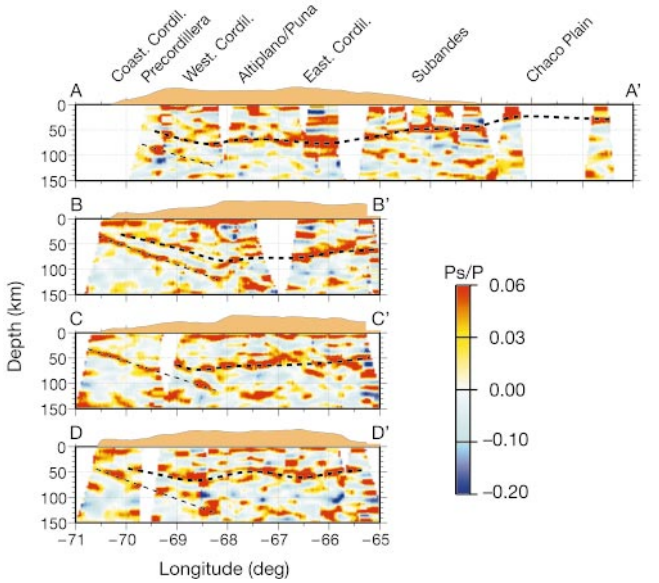

Figure 3 Four east–west depth profiles of migrated RF data within latitude ranges of 1° each. The locations of the profiles are shown in Fig. 1. The surface topography is averaged also within latitude ranges of 1° each. Dashed lines mark the continental and the subducted oceanic Mohos. We note significant uplift of the Moho from the Altiplano (lines A–A′ and B–B′) to the Puna (lines C–C′ and D–D′) at 66–68° W, which is not accompanied by large altitude changes.

together with the smoothed surface topography. Large variations of the depth of the Moho beneath the high plateau indicate strong heterogeneity of the lithospheric thickness, where a thin mantle lithosphere is required to maintain high topography if the crust is thin. This is probably the case for the Puna plateau, in accord with strong lithospheric delamination suggested for this region[15].

The second pronounced feature is the Nazca converter (Fig. 2c), which can be traced parallel to the Wadati–Benioff zone down to a depth of 120 km. Individual P-to-S conversions from the Nazca converter are most clearly seen in records from two earthquakes with relatively flat incidence angles on the subducting plate, in agreement with theoretical expectations[16] (see Fig. 4 and filled circles in Fig. 1 for epicentres). A dominant dipping positive phase (marked black in Fig. 4) crosses the entire CINCA network from 5.5 s to 9.5 s from west to east and continues further eastwards into the centre of the PISCO network at 14.5 s delay time. (The locations of the CINCA and PISCO networks are shown in Fig. 1.) About 1.3 s earlier than the positive phase, there is a clear correlatable negative phase, which cannot be interpreted as a side lobe of the P signal because it is too large and appears only on one side of the positive phase.

The RF waveforms can be modelled by a low-velocity layer, 5–10 km thick, with an S-wave velocity contrast of about 15% (inset in Fig. 4). This layer thickness and velocity contrast to the surrounding mantle corresponds to non-eclogitized mafic oceanic crust versus garnet peridotite[17]. In this case, the Nazca converter represents the Moho of the subducted oceanic crust. As seen from Fig. 2c, the Nazca converter is exceptionally 'bright' down to a depth of about 120 km, where it terminates abruptly. The probable cause of such a breakdown is completion of the gabbro to eclogite transformation in most of the oceanic crust, which would make it seismically almost indistinguishable from the peridotitic mantle[17]. As eclogite is the thermodynamically stable modification of both water-containing and dry mafic rocks at depths greater than 80 km (ref. 18), observation of non-eclogitized crust deeper than 80 km provides direct evidence for kinetically delayed metamorphic reactions in the subducting plate—such reactions have been invoked previously to explain intermediate depth earthquakes[19].

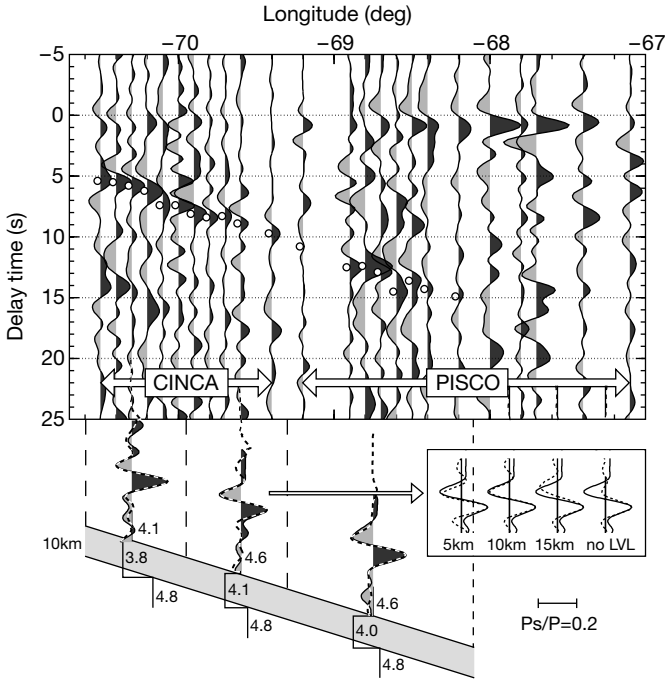

Figure 4 RFs from two earthquakes (filled circles in Fig. 1) recorded by the CINCA and PISCO seismic networks and their modelling. Single RFs are sorted from west to east by the geographical longitude of stations and stacked in bins of 10 km. A 2–10-s bandpass filter is applied to the data. P-to-S conversions can be clearly traced from 5.5 s to 14.5 s time. Positive amplitudes of the converted waves (black) are coherently preceded by negative amplitudes (grey). Stacked RF waveforms can be modelled by the response of a 5–10-km-thick layer with a reduction of S-wave velocity of about 15% relative to the surrounding mantle. A model without a low-velocity layer (LVL) is unable to explain the large negative signals in front of the positive Nazca converter.

The migrated RF image (Fig. 2c) of the subducting crust addresses directly the question of whether intermediate earthquakes are located within the crust or not. High-precision earthquake locations in the Central Andes between 22° and 24° S are also shown in Fig. 2c. Most of the events are located within the oceanic crust which is still not completely eclogitized, but the lower part of the middle section of the cluster extends below the oceanic crust by some 10–20 km. This observation differs from the situation at 21° S, where most of the cluster is apparently shifted into the oceanic mantle, as reported by a deep reflection study[20]. Most of the intermediate depth seismicity, as well as the RF image of incompletely eclogitized crust, terminates where a conspicuous increase in subduction angle occurs. This may be an additional indication of the same reaction-driven processes within the slab. In this case enhancement of slab pull following the completion of eclogitization and/or decrease of oceanic crustal strength due to the continuing dehydration may control this feature.

Two clear intracrustal converters TRAC1 and TRAC2 (Fig. 2a–c) confine a low-velocity zone (hereafter called the Andean low-velocity zone, ALVZ). The ALVZ crosses the entire Altiplano/Puna plateau from the Eastern Cordillera to the Western Cordillera, dipping slightly to the west, and is characterized by a reduction of seismic wave velocity of about 10–20% (see Fig. 2b). Locally, this reduction is even higher, with the highest values below major ignimbrite fields (Supplementary Information, Fig. S2). The existence of the extended low-velocity zone was previously reported from wide-angle reflection studies along several lines crossing the Central Andes[4]. From clear data of P-to-S conversions and their multiples (Supplementary Information, Fig. S3), we estimate the average crustal v_P/v_S ratio to be about 1.80 in the southern Altiplano and Puna (here v_P and v_S are the velocities of P and S waves, respectively). This value of 1.80 is much larger than the value of 1.70 that is expected for solid elastic rocks having v_P values less than 6.3 km s^{-1} in the α-quartz stability field[17]. This indicates some significant non-lithological effects on seismic velocities, or very high temperatures (β-quartz stability). To the north of 22° S (see Supplementary Information, Fig. S2), the ALVZ is also evident but is weaker, in accord with a lower v_P/v_S ratio observed there[5,6].

Due to the clear correlation of the ALVZ strength with volcanic activity (Fig. S2, Supplementary information) and high v_P/v_S ratio, we interpret the ALVZ as a high-temperature zone with partial melting achieved in the places of strongest conversions (Supplementary Information, Fig. S2) and continuing prograde metamorphic reactions in the rest of it. The thermal conditions needed for this feature are most probably caused by mantle magmatism and heat advection (related to subduction, lithospheric mantle delamination[15] and intracrustal diapirism), as thickening of radiogenic crust and shear heating could not have achieved mid-crustal melting since the Miocene epoch. Hot lower crust before shortening, as indicated from xenolith data of crust originally located to the east of the Eastern Cordillera[21], may have supported this evolution. In this interpretation, the top of the ALVZ (TRAC1 boundary) represents the upper limit of compaction-porous vertical flow of fluids and melts associated with the present brittle–ductile transition in the upper crust. Melt accumulation along this boundary may produce huge partial-melt bodies[22] (see also Supplementary Information, Fig. S2). The bottom of the ALVZ (TRAC2 boundary) may represent the upper boundary of the dry and hot refractory lower crust, which has already lost melts and volatiles and therefore obtained higher seismic velocities.

Moreover, the direct link of the ALVZ to the basal detachment under the eastern plateau margin, as well as its correlation with the extent of the entire shortened plateau upper crust (Fig. 2), strongly supports its relevance to the tectonic shortening process. The mechanical weakness of the mid-crustal ALVZ and the Eastern Cordillera basal detachment, as inferred from the presence of melts and fluids, probably separates crustal shortening in an upper-crust imbricate belt[7–9] from a deeper crust with an unknown mode of internal deformation. The continuity of the deep crustal structure across the entire plateau suggests a single crustal thickening process, namely tectonic shortening, rather than important additional contributions from other processes that involve the mantle[23]. As a consequence, bulk crustal shortening from surface observations may have been substantially underestimated.

Our interpretation of the ALVZ is similar, in its tectonic aspect, to the interpretation of the low-velocity zone in Tibet—which has remarkably similar depth, thickness and lateral extent[24,25]. Moreover, as documented by a study of xenoliths[26], the middle crust (30–50 km depth) of the northern Tibetan plateau consists of hot and dry refractory rocks similar to those we expect below TRAC2. The existence of analogous low-velocity zones below the Earth's two highest plateaux suggests their fundamental role in the plateau-building process, possibly as decoupling zones that partition crustal shortening into a largely brittle upper-crust domain and ductile deep crust. □

Received 15 October 1999; accepted 12 October 2000.

1. DeMets, C., Gordon, R. G., Argus, D. F. & Stein, S. Current plate motions. *Geophys. J. Int.* **101,** 425–478 (1990).
2. Isacks, B. L. Uplift of the central Andean plateau and bending of the Bolivian orocline. *J. Geophys. Res.* **93,** 3211–3231 (1988).
3. James, D. E. Andean crustal and upper mantle structure. *J. Geophys. Res.* **76,** 3246–3271 (1971).
4. Wigger, P. J. *et al.* in *Tectonics of the Southern Central Andes* (eds Reutter, K. -J., Scheuber, E. & Wigger, P. J.) 23–48 (Springer, Berlin, 1994).
5. Zandt, G., Velasco, A. A. & Beck, S. L. Composition and thickness of the southern Altiplano crust, Bolivia. *Geology* **22,** 1003–1006 (1994).
6. Beck, S. L. *et al.* Crustal thickness variations in the Central Andes. *Geology* **24,** 407–410 (1996).
7. Allmendinger, R. W. & Gubbels, T. Pure and simple shear plateau uplift, Altiplano-Puna, Argentina and Bolivia. *Tectonophysics* **259,** 1–13 (1996)
8. Kley, J. & Monaldi, C. R. Tectonic shortening and crustal thickness in the central Andes: how good is the correlation? *Geology* **26,** 723–726 (1998).
9. Lamb, S., Hoke, L., Kennan, L. & Dewey, J. in *Orogeny Through Time* (eds Burg, J. P. & Ford, M.) 237–264 (Special Publication 121, Geological Society, London, 1997).
10. Allmendinger, R. W., Jordan, T. E., Kay, S. M. & Isacks, B. L. The evolution of the Altiplano-Puna Plateau of the Central Andes. *Annu. Rev. Earth Planet. Sci.* **26,** 139–174 (1997).
11. Owens, T. J., Zandt, G. & Taylor, S. R. Seismic evidence for an ancient rift beneath the Cumberland Plateau, Tennessee: A detailed analysis of broadband teleseismic P waveforms. *J. Geophys. Res.* **89,** 7783–7795 (1984).
12. Yuan, X., Ni, J., Kind, R., Mechie, J. & Sandvol, E. Lithospheric and upper mantle structure of southern Tibet from a seismological passive source experiment. *J. Geophys. Res.* **102,** 27491–27500 (1997).
13. Jones, C. H. & Phinney, R. A. Seismic structure of the lithosphere from teleseismic converted arrivals observed at small arrays in the southern Sierra Nevada and vicinity, California. *J. Geophys. Res.* **103,** 10065–10090 (1998).
14. Kosarev, G. *et al.* Seismic evidence for a detached Indian lithospheric mantle beneath Tibet. *Science* **283,** 1306–1309 (1999).
15. Kay, R. W. & Kay, S. M. Delamination and delamination magmatism. *Tectonophysics* **219,** 177–189 (1993).
16. Cassidy, J. F. Numerical experiments in broadband receiver function analysis. *Bull. Seismol. Soc. Am.* **82,** 1453–1474 (1992).
17. Sobolev, S. V. & Babeyko, A. Yu. Modelling of mineralogical composition, density and elastic wave velocities in the unhydrous rocks. *Surv. Geophys.* **15,** 515–544 (1994).
18. Peacock, S. M. The importance of blueschist - eclogite dehydration reactions in subducting oceanic crust. *Geol. Soc. Am. Bull.* **105,** 684–694 (1993).
19. Kirby, S., Engdahl, E. R. & Denlinger, R. in *Subduction Top to Bottom* (eds Bebout, G. E., Scholl, D. W., Kirby, S. H. & Platt, J. P.) 195–214 (Geophysical Monograph 96, American Geophysical Union, Washington DC, 1996).
20. ANCORP Working Group. Seismic reflection image of Andean subduction zone revealing offset of intermediate-depth seismicity into oceanic mantle. *Nature* **397,** 341–344 (1999).
21. Lucassen, F., Lewerenz, S. & Franz, G. Metamorphism, isotopic ages and composition of lower crustal granulite xenoliths from the Cretaceous Salta Rift, Argentina. *Contrib. Mineral. Petrol.* **134,** 325–341 (1999).
22. Chmielowski, J., Zandt, G. & Haberland, C. The central Andean Altiplano-Puna Magma body. *Geophys. Res. Lett.* **26,** 783–786 (1999).
23. Giese, P., Scheuber, E., Schilling, F., Schmitz, M. & Wigger, P. Crustal thickening processes in the Central Andes and the different natures of the Moho-discontinuity. *J. S. Am. Earth Sci.* **12,** 201–220 (1999).
24. Nelson, K. D. *et al.* Partially molten middle crust beneath southern Tibet: Synthesis of project INDEPTH results. *Science* **274,** 1684–1688 (1996).
25. Kind, R. *et al.* Evidence from earthquake data for a partially molten crustal layer in southern Tibet. *Science* **274,** 1692–1694 (1996).
26. Hacker, B. R. *et al.* Hot and dry deep crustal xenoliths from Tibet. *Science* **287,** 2463–2466 (2000).
27. Cahill, T. A. & Isacks, B. L. Seismicity and shape of the subducted Nazca Plate. *J. Geophys. Res.* **97,** 17503–17529 (1992).
28. Graeber, F. & Asch, G. Three dimensional models of P wave velocity and P to S velocity ratio in the southern central Andes by simultaneous inversion of local earthquake data. *J. Geophys. Res.* **104,** 20237–20256 (1999).
29. Engdahl, E. R., van der Hilst, R. D. & Buland, R. Global teleseismic earthquake relocation with improved travel times and procedures for depth determination. *Bull. Seismol. Soc. Am.* **88,** 722–743 (1998).

Supplementary information is available on *Nature*'s World-Wide Web site (http://www.nature.com) or as paper copy from the London editorial office of *Nature*.

Acknowledgements

We thank R. Trumbull and F. Lucassen for discussions, J. Mechie and D. Harlov for comments on the manuscript, and G. Chong and M. Wilke for supporting the experiments. The field experiments were supported by the Collaborative Research Center (SFB) 267 of the Deutsche Forschungsgemeinschaft, the GeoForschungsZentrum Potsdam, the Freie Universität Berlin, the US National Science Foundation, the PASSCAL project, the Universidad de Chile (Santiago) and the Universidad Catolica del Norte (Antofagasta).

Correspondence and requests for materials should be addressed to R.K. (e-mail: kind@gfz-potsdam.de).

Disturbance and diversity in experimental microcosms

Angus Buckling*, Rees Kassen†, Graham Bell†‡ & Paul B. Rainey*

* *Department of Plant Sciences, University of Oxford, Oxford OX1 3RB, UK*
† *Department of Biology, McGill University, Montreal H3A 1B1, Quebec, Canada*
‡ *Redpath Museum, McGill University, Montreal H3A 2K6, Quebec, Canada*

External agents of mortality (disturbances) occur over a wide range of scales of space and time, and are believed to have large effects on species diversity. The "intermediate disturbance hypothesis"[1–3], which proposes maximum diversity at intermediate frequencies of disturbance, has received support from both field[4,5] and laboratory[6,7] studies. Coexistence of species at intermediate frequencies of disturbance is thought to require trade-offs between competitive ability and disturbance tolerance[8], and a metapopulation structure, with disturbance affecting only a few patches at any given time[9–11]. However, a unimodal relationship can also be generated by global disturbances that affect all patches simultaneously, provided that the environment contains spatial niches to which different species are adapted[12]. Here we report the results of tests of this model using both isogenic and diverse populations of the bacterium *Pseudomonas fluorescens*. In both cases, a unimodal relationship between diversity and disturbance frequency was generated in heterogeneous, but not in homogeneous, environments. The cause of this relationship is competition among niche-specialist genotypes, which maintains diversity at intermediate disturbance, but not at high or low disturbance. Our results show that disturbance can modulate the effect of spatial heterogeneity on biological diversity in natural environments.

Selection in heterogeneous environments may act to maintain diversity[13–15], and the conditions under which this can occur have recently been derived[16] using a modification of the classic Levene model[17]. There are two key requirements. First, each species must be fitter than the other in one of the two niches, so that selection is antagonistic. Second, each niche must contribute approximately equal numbers of individuals to the global population. If one niche contributes many more individuals to the community than the